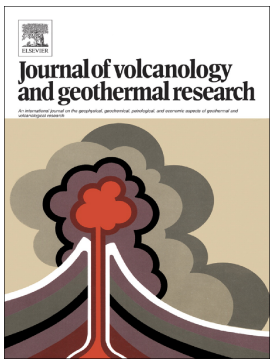

Liquid jet breakup regimes in lava fountains

Pier Paolo Comida, Pierre-Simon Ross, Bernd Zimanowski, Ralf Büttner, Ingo Sonder

PII: S0377-0273(22)00140-8

DOI: https://doi.org/10.1016/j.jvolgeores.2022.107609

Reference: VOLGEO 107609

To appear in: *Journal of Volcanology and Geothermal Research*

Received date: 3 August 2021

Revised date: 9 June 2022

Accepted date: 13 June 2022

Please cite this article as: P.P. Comida, P.-S. Ross, B. Zimanowski, et al., Liquid jet breakup regimes in lava fountains, *Journal of Volcanology and Geothermal Research* (2022), https://doi.org/10.1016/j.jvolgeores.2022.107609

Liquid jet breakup regimes in lava fountains

Pier Paolo Comida[1,*] pier_paolo.comida@inrs.ca, Pierre-Simon Ross[1] pierre-simon.ross@inrs.ca, Bernd Zimanowski[2] zimano@mail.uni-wuerzburg.de, Ralf Büttner[2] buettner@mail.uni-wuerzburg.de, Ingo Sonder[3] ingomark@buffalo.edu

[1]Institut national de la recherche scientifique, 490 rue de la Couronne, Québec (Qc), G1K 9A9, Canada
[2]Physikalisch Vulkanologisches Labor, Universität Würzburg, Pleicherwall 1, 97070, Würzburg, Germany
[3]Center for Geohazards Studies, University at Buffalo, 126 Cooke Hall, Buffalo, NY 14260, United States

[*]Corresponding author.

Abstract

Primary magma fragmentation in "fluid-dominated" (as opposed to "ash-dominated") lava fountains involves the hydrodynamic breakup of a jet of magma. Lava fountains partly resemble industrial liquid jets issued from a nozzle into a quiescent atmosphere, on which there is a vast literature. Depending on the internal liquid properties, nozzle diameter and ejection velocity, liquid jet breakup in industrial applications occurs in four regimes: (I) coarse laminar breakup (Rayleigh regime); (II) transition region between laminar and turbulent breakup (first wind-induced regime); (III) turbulent breakup at the jet surface and unstable but intact liquid core (second wind-induced regime); (IV) fully turbulent fine spray (atomization regime).

Ductile magma breakup associated with regimes II, III and IV have been reproduced during the initial expansion of experimental magma fragmentation

pulses as part of this study. In each experiment, volcanic rocks were re-melted at 1200°C, then fragmented through the injection of compressed argon gas within a few tens of milliseconds. Three compositions were used: olivine-melilitite, alkali basalt, and basaltic trachy-andesite. Each composition was ejected at 3 and 10 MPa gas driving pressure, yielding exit velocities between 11–13 and 33–44 m/s, respectively. The ultramafic magma ejected at high speed developed quickly into a fully developed spray (regime IV), whereas the basaltic trachy-andesite ejected at low-speed initially expanded as a coherent magma mass before breaking into coarse domains (regime II). The observed variability among the experiments is linked to the relative balance among surface tension, viscosity, density, jet diameter and ejection velocity of the magma versus external aerodynamic effects acting on the jet surface. These factors, particularly viscosity and exit velocity, are also likely to control jet breakup regimes in natural lava fountains and some Strombolian pulses.

Keywords: hydrodynamic breakup; magma fragmentation; lava fountains; fragmentation experiments; breakup regimes

1. Introduction

Hawaiian style lava fountains are a common type of subaerial eruption (Parfitt and Wilson, 2009; Taddeucci et al., 2015). These fountains typically involve volatile-rich mafic magmas, last several minutes to several days, and consist of jets that can rise from meters to several hundred meters into the atmosphere (Cashman and Scheu 2015; Taddeucci et al., 2015; Calvari et al., 2018; Mueller et al., 2018). La Spina et al. (2021) distinguish lava fountains as “fluid-dominated”, when mainly

characterized by ductile (hydrodynamic) fragmentation, and “ash-dominated”, when more ash is generated through brittle fragmentation. Since our experiments reproduced hydrodynamic breakup processes, this work focuses on “fluid-dominated” lava fountains.

Lava fountains can be seen as a natural example of liquid jet breakup (Eggers and Villermaux, 2008). There is a vast literature on the hydrodynamic breakup of liquid jets in industrial and commercial applications, such as ink jet printers or diesel engines. This previous work has shown that four jet breakup regimes exist, ranging up to full sprays; the controls on these regimes are well known (Reitz and Bracco, 1986; Eggers and Villermaux, 2008; Biroul and Lekic, 2009; Lefebvre and McDonell, 2017 and references therein).

This study aims to better understand controls on lava fountains by comparing them with jet breakup phenomena documented for industrial applications. We introduce a modified version of the Ohnesorge diagram and illustrate the effect of changing each of the important parameters. We then present ejection experiments involving fragmentation of remolten volcanic rocks (referred as to informally “magma” for simplicity); these experiments resemble lava fountain pulses. We changed only two parameters, magma composition and ejection velocity, between each run, but accessed three of the four regimes of jet breakup. Those same three regimes also appear to be present in examples of natural lava fountains.

The rest of this paper is organized as follows. We start with a review of liquid jet breakup mechanisms and regimes in industrial and commercial applications (section 2). In the methods (section 3), the tested materials and experimental setup

are presented. Next comes the description of the physical properties of the magmas (section 4). In section 5, the results of the experiments are presented, using the high-speed video footage. Finally, section 6 discusses the similarities between industrial liquids jets and our magma jets, before drawing a comparison with natural lava fountains.

2. Review of liquid jet breakup in industrial and commercial applications

The breakup of liquid jets ejected from a nozzle has been the subject of scientific research for over 130 years, vastly exploited for several industrial and commercial applications (Eggers and Villermaux, 2008; Birouk and Lekic, 2009; Lefebvre and McDonell, 2017). The studied fluids span different rheological behaviors (e.g. inviscid, Newtonian and non-Newtonian), viscosities over several orders of magnitude and varied ejection velocities (McCarthy and Molloy, 1974; Reitz and Bracco, 1986; Eggers and Villermaux, 2008; Birouk and Lekic, 2009; Clasen et al., 2012; Lefebvre and McDonell, 2017). There are also different ejection configurations: classic studies involved liquids issued vertically downward into a quiescent atmosphere, although other setups have also been used (Eggers and Villermaux, 2008; Wang et al., 2012; Jones et al., 2019). Beyond the internal properties of the liquid jet and its flow regime before and at the nozzle exit, the shape of the nozzle and the characteristics of the surrounding medium are the other main control factors dictating the disintegration of a liquid jet. The surrounding medium, when involving gasses, can be of three types: i) quiescent air/gas (Reitz and Bracco, 1986; Chigier and Reitz, 1996); ii) a coaxial flow issued

from an annular orifice fixed around the liquid nozzle, ejecting gas in the same direction as the liquid jet (Chigier and Reitz, 1996); iii) a crossflow which blows air/gas perpendicularly to the liquid jet ejection axis (Sallam et al., 2004; Cao et al., 2007).

2.1. Why liquid jets break up

Given the very large number of combinations of ejected liquid properties and surrounding medium configurations, a unified description of the breakup process is not possible. For the purpose of assessing the jet breakup mechanisms in our experiments and in nature, we consider in the rest of this section the basic downward ejection of a liquid jet from a long pipe at constant velocity into quiescent air at atmospheric pressure (Birouk and Lekic, 2009; Lefebvre and McDonell, 2017). As the jet moves away from the nozzle, the competition between forces within the liquid and external aerodynamic forces at the jet surface will generate wave-like disturbances. Once a critical wave amplitude is reached, the liquid jet breaks up into filaments and drops; this is known as primary breakup. Secondary breakup of the newly formed drops and threads into smaller fragments might occur if the primary drops are still large enough (Birouk and Lekic, 2009; Lefebvre and McDonell, 2017), and sufficient time and travel distance are given. In a state of equilibrium, the internal pressure distributed at the liquid surface is equal to the sum of external aerodynamic and surface tension pressures (Lefebvre and McDonell, 2017). As the latter is inversely proportional to the drop size, aerodynamic effects acting on a relatively large liquid drop will be stronger than

surface tension pressures, leading to deformation and breakup. As the newly formed drops become progressively smaller, surface tension pressure will increase relative to the aerodynamic pressures, until the critical drop size is reached. Beyond this size, surface tension pressures will be able to accommodate any destabilizing effect by aerodynamic forces, and no further breakup will occur (Lefebvre and McDonell, 2017).

2.2. Jet breakup regimes

Several time and length scales are related in a complex manner during the breakup process of liquid jets. Time scales of early thinning and breakup of an initially coherent liquid volume into threads or drops varies strongly depending on the liquid's material properties, the ejection velocity, and the surrounding medium. The disintegration may affect the whole mass at once, or it may be initially limited to the surface of the jet. Over the past four decades, the investigation into this variety of conditions has led to the identification of different breakup regimes. Several regime classifications have been used. Since each regime is generally defined by a similar set of conditions regardless of the classification method, we will briefly introduce the main two classifications before describing each regime.

2.2.1. Jet stability curve classification

The relationship between ejection velocity and the intact length of the liquid jet (distance from the nozzle exit to the point of primary breakup) constitutes the basis of the stability curve classification of jet breakup regimes (Fig. 1a). For the simplest case of a liquid issued downward into the atmosphere, a progressive shift in the

expansion and fragmentation of the liquid is observed when increasing ejection velocity (Fig. 1b). At the lowest ejection velocity, the liquid jet is unable to form a coherent liquid jet and breaks up into drops upon exiting the nozzle because of liquid inertia and surface tension; this is known as the dripping region (not shown). For larger ejection velocities, a fully formed liquid jet is established and four main breakup regimes exist, as described below.

2.2.2. Ohnesorge classification

The velocity of the liquid influences its internal flow regime (i.e. laminar, semiturbulent or turbulent) before it emerges from the nozzle, contributing to its final disintegration once in the air, along with aerodynamic forces. A low velocity will favor a laminar regime, along with the absence of any asperity inside the pipe (Lefebvre and McDonell, 2017). Increasing liquid velocity and pipe roughness will instead enhance liquid instability, favoring a turbulent regime.

When a liquid is injected inside a pipe, its velocity profile (and flow regime) is not instantaneously fully developed, and it takes some time before it reaches that state. At the inlet of the pipe we have a “hydrodynamic entrance region”, where the velocity profile of the liquid is not yet developed because of viscous forces in the liquid are enhanced by the wall of the pipe. The length of the hydrodynamic entrance region can be estimated for cylindrical pipes as function of Re (even for the turbulent case). By flowing towards the outlet of the pipe (i.e., the nozzle), the liquid progressively stabilizes until the velocity profile is fully developed; this is known as the “fully developed region”. In classic atomization experiments, a long

tube is normally used to ensure the stability of the liquid within a specific regime before it emerges from the nozzle.

The development of internal disturbances within the liquid jet also depends on its internal properties; liquids with different densities (ρ), viscosities (η) and surface tensions (σ) issued with the same velocity (u) will break up differently from one another. During the flow of liquid jets, aerodynamic pressures at the air-liquid interface compete with internal pressures (dependent on physical properties of the liquid such as surface tension and viscosity), deforming the liquid surface (Lefebvre and McDonell, 2017). If aerodynamic forces dominate over surface tension, this state of disequilibrium ultimately leads to the breakup of the jet. These variables are typically combined into two dimensionless parameters, the Reynolds number for Newtonian viscosities $\mathrm{Re} = \frac{\rho v d}{\eta}$ and the Weber number $\mathrm{We} = \frac{\rho v^2 d}{\sigma}$, where d is a characteristic length usually represented by the nozzle diameter. Both Re and We quantify the relative importance of a fluid's inertia, relative to its viscosity and surface tension, respectively. A third dimensionless parameter widely used in jet breakup studies, the Ohnesorge number, is a ratio of the first two: $\mathrm{Oh} = \frac{\sqrt{We}}{Re} = \frac{\eta}{\sqrt{\rho \sigma d}}$. The traditional Ohnesorge diagram plots Oh versus Re and shows the four breakup regimes (Fig. 1c).

On this diagram, viscosity has opposite effects on Oh versus Re, making it difficult to visualize the effect of viscosity on regime changes. Since viscosity is a very relevant parameter when dealing with magmas, we introduce an alternative way

to assess regime transitions in liquid jet breakup, obtained by comparing We and Re (Fig. 1d). Now the viscosity appears only in the x axis, so increasing the viscosity produces a simple leftward trend on the diagram, progressively crossing regime boundaries. The regime boundaries in this new diagram decay with $We \sim Re^{-0.5}$.

2.2.3. The four jet breakup regimes

The four main jet breakup regimes are, for increasing ejection velocities:

I. Laminar flow region of the stability curve classification (Rayleigh's regime in the Ohnesorge classification) – At relatively low ejection velocity, the liquid jet is initially in a predominant laminar flow state. Surface tension and liquid inertia dominate the breakup process, with negligible aerodynamic effects, resulting in small surface disturbances that fragment the liquid jet into drops (regime I on Fig. 1). In this regime, there is a direct relationship between longer threads and ejection velocity. After breakup, the width of the drop might be generally larger than the nozzle diameter but within the same order of magnitude.

II. Transition region (first wind-induced regime) – At higher ejection velocity, the liquid jet develops internal turbulence that is transmitted towards the gas-liquid interface. Aerodynamic effects are no longer negligible, enhancing wave disturbances at the liquid surface that contribute to the ultimate breakup of the jet (regime II in Fig. 1). This regime is characterized by an inverse relationship between ejection velocity and intact length of the liquid jet. The size of the newly formed fragments is still within the same

order of magnitude as the initial liquid jet, and breakup still occurs at a certain distance from the nozzle exit.

III. Turbulent flow region (second wind-induced regime) – In this regime, aerodynamic forces at the gas-liquid interface become important on the breakup process, relative to internal turbulence in the liquid jet. Surface wave disturbances cause the disintegration of the liquid jet relatively closer to the nozzle exit, although there is still an intact (unfragmented) portion to the jet near the nozzle. The length of the drops tends to again increase with increasing velocity (regime III in Fig. 1a). The size of the newly formed drops is now much smaller than the nozzle diameter (Fig. 1b).

IV. Fully developed spray region (atomization regime) – At extremely high ejection velocities (up to, and beyond the speed of sound), the flow is fully turbulent. Also, strong aerodynamic forces at the jet front cause the violent disintegration of the liquid jet very close to the nozzle. The length of the newly formed drops progressively decreases with increasing ejection velocity (regime IV in Fig. 1), and their size will be up to several orders of magnitude smaller than the nozzle diameter (Fig. 1b).

Regime transitions can also be obtained by keeping the velocity constant but changing one of the other main parameters. Increasing either the liquid density or the nozzle diameter leads to both higher We and Re, promoting the fine disintegration of the liquid jet (Fig. 1d). Increasing surface tension leads to a lower We, shifting the jet towards the Rayleigh regime. Increasing viscosity reduces Re, again enabling the transition toward the Rayleigh regime (Fig. 1d).

3. Methods

Magma fragmentation experiments were carried out at the *Physikalisch Vulkanologisches Labor* (PVL) in the University of Würzburg (Germany). Discrete upward moving pulses of artificial 'magma' were produced and filmed. This allowed access to three breakup regimes (II, III and IV).

3.1. Tested materials

The magmas fragmented in the experiments were generated from three volcanic rock materials, ranging from ultramafic to intermediate compositions (Fig. 2a). They include: i) Hohenstoffeln, a dense olivine-melilitite with ~ 38 wt.% SiO_2 from a lava lake in the Tertiary Hegau volcanic field in Germany (Zimanowski et al., 1997; Hobiger et al., 2011); ii) Bilstein, a thick and dense alkaline basalt lava flow with ~ 45 wt.% SiO_2 from the Rhön volcanic field, Germany (Zimanowski et al., 2004; Dürig et al. 2012); iii) Sommata, a basaltic trachyandesite lapilli-size scoria deposit with ~ 54 wt.% SiO_2 from the island of Vulcano in the Aeolian archipelago, Italy (Büttner et al., 2002; Hobiger et al., 2011; De Astis et al., 2013). Despite the Sommata material being scoriaceous, after remelting it also produced a dense (bubble-poor) magma, like the other two materials. All the original rock materials contained a variable amount of phenocrysts, at least some of which survived the re-melting process (see below).

3.2. Experiment setup and timeline

The selected volcanic rocks were re-melted and then fragmented using two different experimental setups. The reason for using two different setups is that these experiments were part of a larger program, which also involved phreatomagmatic experiments. Out of this larger program, for this paper, we selected six successful gas-driven hydrodynamic fragmentation runs covering three magma compositions and two driving pressures.

Regardless of the experiment configuration (detailed below), preparation for each run involved placing a set amount of granulated rock inside a 5 cm (inner diameter) steel crucible. The granules were heated to 1200°C within one hour, using an induction furnace (Figs. 2b, c). Such rapid heating might leave some crystals in the magma.

The first experimental setup, informally known as the “blowout” (detailed in Büttner et al., 2006), was used for the “high speed” runs (Fig. 2b). About 200 g of granulated material was employed in each run. A fixed volume of compressed argon at 10 MPa (100 bars) was suddenly introduced through a hole at the base of the crucible by opening a valve. This rapidly pushed the magma upward as a plug, causing hydrodynamic fragmentation at the gas-magma plug interface within the crucible. In almost all the experiment runs, the arrival of the magma plug at the crucible opening coincided with the argon gas laterally piercing through the magma, leading to droplet generation (Fig. 2d). As will be seen below, this gas piercing phase is relatively minor in terms of volume of fragmented magma. Further and complete fragmentation of the perturbed magma plug occurred in the

atmosphere, and this is the liquid jet breakup part that we are interested in for this paper.

The other setup ("injection type" configuration; e.g., Zimanowski et al., 1997), was used for the lower pressure experiments (Fig. 2c). Each run employed 255 g (± 10 g) of granulated volcanic rock. A discrete volume of compressed argon gas at 3 MPa (30 bars) was injected directly within the magma through a J-shaped steel pipe mounted on a servo drive. The injected gas pushed the magma upwards, again causing expansion and hydrodynamic fragmentation both within the crucible and in the atmosphere (Zimanowski et al., 1997). For both setups, ejection from the crucible and associated fragmentation of the magma was completed within 50 and 80 ms, respectively.

3.3. Video footage analysis

The free air fragmentation phase of each run was recorded using high-speed cameras, as detailed in Zimanowski et al. (1997). We employed 2000 and 5000 frames per second to capture the 10 MPa and 3 MPa series, respectively. The experiments were also filmed from various angles using regular video cameras. Repulsion force and pressure were recorded.

Analysis of the high-speed video footage allowed to investigate thinning and breakup processes of the magma during each run. The average ejection velocity of the coherent magma plug was tracked at the crucible exit using a combination of Adobe Illustrator® and Phantom Camera Control (PCC) software®. The

measurements were obtained by tracking the visible, coherent portion of the magma plug at the beginning of the free air expansion, over a time interval of 1.5 ms. The travelled distance corresponded to three and about seven frames, respectively for the 10 MPa and 3 MPa series. The minor gas piercing phase had a much higher velocity but this is not relevant for studying liquid jet breakup regimes.

4. Experimental parameters and physical properties of the magmas

Similar to industrial liquids, jet breakup in magma is governed by its main internal properties, and the violent interaction of the magma with a quiescent atmosphere, influenced by ejection velocity.

4.1. Temperature

Magma temperature greatly influences viscosity, and to a lesser extent density and surface tension (Walker and Mullins, 1981; Shimozuru, 1994). All experiments were carried out at the same initial temperature of 1200°C.

4.2. Crystallinity and bubbles

An estimate on the amount of crystals present in our magmas just before the onset of the experiments comes from the analysis of 2D cross-sectional slices of quickly cooled ash particles. Average crystallinity for our six samples ranges from 0 to ~ 9

vol.%. Similarly, the average amount of bubbles in the magmas was low (0.9-18.7%). A detailed characterization of the crystals and bubbles in the artificial pyroclasts will be provided by Comida et al. (*in prep.*). These narrow intervals are unable to explain the dramatic change in fragmentation behavior observed during the experiments.

4.3. Ejection velocity

By using two driving pressures for each of the tested magmas, we anticipated that each driving pressure would correspond to a certain ejection velocity for all magmas. Indeed, the coherent portion of each magma plug considered in this study shows roughly similar exit velocities for a certain driving pressure (Table 1). The average exit velocity of the 10 MPa series is 38 m/s, which is 3.2 times faster than that of the 3 MPa series (~ 12 m/s).

4.4. Surface tension

Available empirical σ values for Hohenstoffeln and Billstein (Koopmann, 2004) along with another basalt and some more felsic compositions (Murase and McBirney, 1973; Walker and Mullins, 1981) are presented in Fig. 3a. At 1200°C, all of these magmas have surface tensions between ~ 330 and 350 mN/m, a very limited range. So differences in surface tension must not be the controlling factor in explaining the different fragmentation behavior of our three magmas.

4.5. Bubble-free density

The available bubble-free density (ρ) data for two of our tested magmas, along with other compositions, are presented in Fig. 3b. Hohenstoffeln (olivine-melilitite) and Sommata (basaltic-trachyandesite) range between ~ 2920 and ~ 2500 kg/m^3 at 1200°C (Büttner et al., 1998, 2002), and Billstein is assumed to have an intermediate density value, similar to the Galápagos olivine basalts (Fig. 3b). Again, this is a limited range. In our experimental magmas, the average vesicularities only account for few vol. %, therefore density does not explain the different fragmentation behavior.

4.6. Viscosity

Unlike the previous parameters, η can vary by several orders of magnitude between different magmas. Therefore, it has the potential to be one the main factors controlling jet breakup processes (Clasen et al., 2012; Lefebvre and McDonell, 2017).

First, even for a specific magma composition, η depends on temperature (Sonder et al., 2006), proportion of bubbles (Wallace et al., 2015), and crystal content and shape (Mader et al., 2013). In our fragmentation experiments, however, the target temperature was the same for all magmas (section 4.1), while both crystal and bubble contents of the tested magmas were low (section 4.2), therefore accounting for only minor effects on viscosity.

Second, magmas behave as non-Newtonian (shear-thinning) fluids, where η is dependent of the shear rate ($\dot{\gamma}$) at a certain temperature (Sonder et al., 2006; Hobiger et al., 2011). This non-linear dependency is expressed as $\tau = \eta_0 \dot{\gamma}^m$, where *m* is the power-law coefficient for a specific non-Newtonian material at a given temperature and η_0 is the consistency (which differs from viscosity by the power of *m*). For shear-thinning fluids, *m* is less than 1, approaching 1 at increasing temperatures (for reference, *m* = 1 in Newtonian fluids). All our magmas exhibit shear thinning behavior in viscometry experiments, i.e. equilibrium viscosity decreases with increasing rates of deformation (Sonder et al., 2006, Hobiger et al., 2011). Data from viscometry experiments for our three magmas at 1200°C are reported in figure 3c, with viscosity progressively decreasing from top to bottom in each line because of the increasing shear rate. In particular, at the highest shear rates experienced in viscometry experiments ($\dot{\gamma}$ = ~ 20 s^{-1}, bottom end of each data line in Fig. 3c), η progressively increases with SiO_2, with values of 21, 28 and 45 Pa.s, respectively for Hohenstoffeln, Billstein and Sommata. Since the shear rates during the free air expansion phase are believed to be much higher in the current fragmentation experiments than in viscometry experiments, the shear thinning behavior is likely to become even more pronounced, leading to even more different η values among the magmas, with the lowest for Hohenstoffeln. This is compatible with the different jet breakup regimes (and pyroclast shapes, Comida et al., *in prep*) observed in the experiments, as detailed in the next sections.

5. Magma breakup in experiments

Compared to jet breakup for industrial liquids, the disintegration of the magma plug in our experiments is more complex. First, the magma is ejected from a relatively short crucible as a discrete batch by pressurized gas, whereas classic liquid jets are issued from a long pipe at constant rates over a certain amount of time. In our case, the assumption of a long pipe is not satisfied, so that the velocity profile of the magma plug is not likely to be fully developed when it reaches the crucible opening. Second, our magmas are non-Newtonian liquids. Third, a portion of the magma fragmentation takes place inside the crucible, before the magma even exits it (Caffier, 1998). Fourth, gravity slows down the upward moving magma plug and drops, whereas industrial liquid jets are classically issued downwards. Fifth, the jet breakup of the magma plug and especially the drops beyond the field of view of the high-speed camera will be cooled in the atmosphere, influencing their rheology.

Nonetheless, the physics of jet breakup still applies, allowing a detailed description of the extra-crucible fragmentation process in our experiments. The breakup dynamics of the magma plug immediately above the crucible opening can be regarded, in fact, as the first moment of a sustained liquid jet issued from the nozzle. Despite the discrete supply of magma being ejected from the crucible, the 1.4 height/diameter ratio of the crucible allowed the bulk propulsion of the magma plug with minor deformation (Fig. 4). Moreover, the use of the same crucible size and geometry throughout the entire experiments series imparted same initial configuration, therefore highlighting the role of magma composition and driving

pressure during the early stage of the free-air expansion. The momentum provided by the argon “hammer” to the magma plug results in the hydrodynamic breakup of the material above the crucible, similarly to the onset of a sustained liquid jet. However, since the assumption of a long pipe is not satisfied, the applicability of the jet breakup theory to the intermediate and late stage of the experiments cannot be guaranteed.

In comparison with a natural lava fountain, our experiments are partly similar to a single fragmentation pulse, as discussed further in section 6. There is also an apparent resemblance to Strombolian dynamics, due to the discrete nature of the ejection process and the way the magma is fragmented by gas injection in the crucible. Nonetheless, there are several differences between our experiments and Strombolian-style explosions: i) Magma breakup in the latter occurs through the central rupture of the magma film at the top of a gas slug (Gonnermann 2015), whereas in the experiments the magma exits mostly as a plug which is then fragmented in the atmosphere; ii) the near absence of bubbles within the magma plug in the experiments leads to the exclusive generation of achnelith-like fragments, whereas Strombolian pulses commonly generate scoriaceous particles. Our intent is to compare classic liquid jets to lava fountain pulses. To describe magma breakup in our experiments, we first deal briefly with in-crucible fragmentation, then asses the free-air expansion.

5.1. In-crucible magma fragmentation

The first stage of magma fragmentation in the experiments is in-crucible fragmentation (Zimanowski et al., 1997). The steel crucible is of course opaque, so the video documentation does not cover in-crucible events. However, injection-type runs (Fig. 2c) are similar to molten-fuel coolants (MFCI) experiments, except for the initial fine fragmentation unique to MFCI. So the documentation of MFCI experiments with transparent crucibles (Zimanowski et al., 2015), plus analogue experiments (Zimanowski et al., 1991, 1995, 1997) and theoretical considerations (Reitz and Bracco, 1986; Caffier, 1998; Eggers and Villermaux, 2008; Birouk and Lekic, 2009), help reconstruct in-crucible events for gas-driven hydrodynamic magma fragmentation.

As the pressurized argon gas is injected either at the base of (10 MPa series) or within (3 MPa series) the magma, the latter is pushed upward and laterally against the crucible walls, starting the ejection process (Fig. 4a). Rayleigh-Taylor instabilities form at the interface between the magma and the gas (Fig. 4a) (Zimanowski et al., 1991). The wavelike motion of the unstable magma-gas interface, enhanced by the high density contrast between the two fluids, causes magma droplets to detach once the amplitude reaches a critical level; this is a type of hydrodynamic fragmentation (Caffier, 1998; Eggers and Villermaux, 2008) (Fig. 4b). This process continues either until the magma plug is completely fragmented, or exits the crucible. A certain degree of brittle fragmentation might occur within the crucible at very high driving pressures (Zimanowski et al., 1997). The observed near-absence of primary brittle fragments in the ejecta from the current experiments (Comida et al., *in prep)* indicates either i) experimental conditions

below the critical stress required for brittle fragmentation (Jones et al., 2019), or ii) effective reannealing of small brittle fragments within the hydrodynamic field (Zimanowski et al., 1997).

The amount of fragmentation produced within the crucible depends on ejection velocity and internal magma properties (Zimanowski et al., 1991; Caffier, 1998). For a same magma composition, a larger velocity will enhance in-crucible fragmentation, as the higher acceleration is directly proportional to larger disturbances at the gas-magma interface (Caffier, 1998; Sallam et al., 2004; Lefebvre and McDonell, 2017). For a same ejection velocity, magmas characterized by lower silica contents are also more prone to in-crucible fragmentation, as a lower viscosity enhances surface tension-dominated hydrodynamic breakup (Clasen et al., 2012).

5.2. Free-air expansion and final fragmentation

5.2.1. Preamble

Figures 5 to 10 show the visible portion of the experiments. The initial conditions that cause the magma plug to expand in the atmosphere are acquired during acceleration within the crucible. The violent push exerted by the pressurized argon gas generates internal turbulence within the magma volume, initially partly damped by the confined geometry. Once the front of the magma plug surpasses the crucible opening, the sudden pressure release allows its full expansion. Ideally, the magma plug should expand upward and radially from the crucible opening.

Nevertheless, an uneven spatial distribution of the pressurized argon at the gas-magma interface resulted in the asymmetric uncorking of the magma plug. This gas piercing phase can be observed in both 3 and 10 MPa experiment series (Figs. 5 to 9) except for the Sommata 3 MPa run (Fig. 10), where the more cohesive structure of the magma plug prevented this phenomenon. In the 10 MPa series, the gas piercing phase mostly occurred on the left (relative to the viewing direction of the camera) (see 1 and 2 ms frames in Figs. 5, 7 and 9), whereas in the 3 MPa series the "L" shape of the injection pipe resulted in the rebound and piercing of the gas to the right (see 3 and 1.6 ms frames in Figs. 6 and 8, respectively). In what follows, we ignore these asymmetric uncorking artefacts produced by the gas piercing effect in order to investigate the jet breakup phenomena.

5.2.2. Early stage of the jet

The initial interaction of the still coherent portion of the magma at the non-driven (top) surface is with the stagnant atmosphere. Because of its inertia, the atmosphere starts to impinge on the magma surface, creating Rayleigh-Taylor wave disturbances (Lefebvre and McDonell, 2017). A good example of this process is captured during the Billstein 3 MPa at 5 ms (Fig. 8). Simultaneously, possible internal turbulence within the magma plug transmits to the surface, amplifying the disturbances (Lefebvre and McDonell, 2017). Later on, small drops are finally detached from the magma surface and rapidly propelled in the atmosphere once the amplitude of the wave disturbances reaches a critical level (Eggers and Villermaux, 2008; Birouk and Lekic, 2009; Lefebvre and McDonell,

2017). The amount of early-detached droplets from the plug surface is directly proportional to ejection velocity and inversely proportional to magma viscosity.

The vertical velocities of the magma plug in the early stage of the jet phase are presented in Table 1. At one extreme, the Sommata 3 MPa magma plug exits the crucible as a coherent mass with an average velocity of 13 m/s. The plug expands in the air and beyond the field of view as a mushroom head shape with no relevant detachment of small fragments, except for some fragmentation induced by the magma flowing through the induction coil which extends slightly above the crucible (Fig. 10). On the other hand, the Hohenstoffeln 10 MPa magma plug exits at an average velocity of 44 m/s, and starts fragmenting immediately (Fig. 5).

The visual appearance of the initially coherent portion of the magma plug once it begins to expand in the atmosphere provides a unique opportunity to constrain its breakup regime. Starting with the Hohenstoffeln 10 MPa run, the magma appears to be within regime IV (spray/atomization) (Birouk and Lekic, 2009; Lefebvre and McDonell, 2017), because of the ease with which it breaks up into abundant drops several orders of magnitude smaller than the crucible diameter (Fig. 5, 12–20 ms).

Both Billstein 10 MPa and Hohenstoffeln 3 MPa runs are likely to be somewhere around the IV-III (atomization – second wind-induced breakup) boundary, with the following observable characteristics: i) the size of the abundant detached droplets is still several orders of magnitudes smaller than the magma plug diameter; ii) the intact length is longer than what is observed for the Hohenstoffeln 10 MPa (Fig. 6, 15 ms; Fig. 7, 8 ms).

Compared to what is described above, Sommata 10 MPa and Billstein 3 MPa appear to be completely within regime III, because of the relatively smaller amount of detached drops and the length of coherent strips of magma observable in the video footage (Fig. 8, 5–15 ms; Fig. 9, 12–20 ms). Unlike industrial liquids or our two more mafic magmas, Sommata is much more viscous, and breaks up as threads instead of drops, but this will be discussed in more detail elsewhere (Comida et al., *in prep*).

Finally, Sommata 3 MPa is thought to be well within regime II (first wind-induced breakup), due to the early fully coherent appearance of the magma plug (Fig. 10, 3–10 ms). When that plug eventually starts to disintegrate, some of the initial separating domains are within the same order of magnitude than the crucible diameter (Fig. 10, 15 ms).

These different fragmentation regimes for different runs translate into different grain size distributions, with Hohenstoffeln runs producing finer-grained pyroclasts than Sommata runs (Comida et al., *in prep*). This is due to a shorter time allowed for fragmentation in lower breakup regimes as well as prolonged thinning at higher silica compositions which delays final breakup.

5.2.3. Intermediate and final stages of the jet

In the intermediate stage, further upward and away from the crucible, the magma progressively decelerates due to gravity. Prolonged flow of argon from below continues to provide partial thrust to the yet unfragmented, but unstable, portion of

the magma mass, which moves toward different directions as several lobes or even threads, each one with a different velocity.

The final upward stages of the experiments involve the thinning (stretching) and secondary breakup of the now several thousand newly formed drops and filaments, depending on the magma composition. For the front part of the magma jet, this portion of the fragmentation process occurred outside the field of view of the high-speed camera, but the process can be clearly observed in the tail of the jet (Figs. 5-7-9, 20–32 ms; Figs. 6-8-10, 30–55 ms).

6. Discussion

6.1. Jet breakup regimes in the experiments

In the previous section we visually associated a breakup regime to each of the experimental runs. Observed regimes during initial expansion beyond the crucible range from a spray (regime IV) for Hohenstoffeln at 10 MPa to the first wind-induced breakup regime (regime II) for Sommata at 3 MPa. Only gas driving pressure and remolten material were changed between each run, not the crucible geometry. Therefore, the parameters left that change the Weber and Reynolds numbers, and are suspected to be responsible for the observed variety in breakup regimes, are ejection velocity and magma viscosity.

In order to take into account the non-Newtonian (shear-thinning) nature of our tested magmas, we calculated Reynolds numbers specifically for power-law fluids

(from Madlener et al., 2009): $\mathrm{Re_{pl}} = \frac{\rho \cdot v^{2-m} \cdot d^{m}}{\eta_0} f_m$, with $f_m = \frac{8^{1-m}}{\left(\frac{3 \cdot m+1}{4 \cdot m}\right)^{m}}$. Available *m* values at 1200°C for Hohenstoffeln, Billstein and Sommata magmas are 0.61, 0.56 and 0.89, respectively (Sonder et al., 2006; Hobiger et al., 2011).

For each run, the values of the physical parameters used to compute both We and Re_{pl} are presented in Table 1. We consider the early stage of the free air expansion of the coherent magma plug, so we assume that the relevant characteristic length (i.e., our "nozzle diameter") is the inner diameter of the crucible, 5 cm. We used the same surface tension value for all runs, for simplicity (recall that surface tensions vary very little between magmas, see Fig. 3). Density among the three magmas varies within a limited range. We calculated an overall ejection velocity for the coherent portion of the melt plug, focusing on the first 1.5 ms after a traceable part becomes visible. Magma viscosity is the major unknown, since:

(i) Magmas (especially Hohenstoffeln and Billstein) display non-Newtonian behavior, but there are no instantaneous viscosity measurements at the relevant, very high shear rates (which themselves are unknown).

(ii) A single value of viscosity cannot be assumed for an unstable mass of magma propelled at high speed into the atmosphere. For individual runs, viscosity may be changing over time and space.

For illustration purposes, we used all available rheology data for our magmas generated through viscometry experiments at 1200°C (Sonder et al., 2006; Hobiger et al., 2011). We hope that the correct instantaneous viscosity for each run is within the utilized range, especially close to the highest shear rates, but we

cannot be certain of that. The actual values of viscosity during fragmentation are likely to be, in fact, lower than those attained in the viscometry experiments.

The two dimensionless numbers are plotted in our modified Ohnesorge diagram (Fig. 11). Hohenstoffeln 10 MPa is visually (on the high-speed video) in regime IV (Table 1), and indeed plots there on the We-Re diagram (Fig. 11). Billstein 10 MPa and Sommata 10 MPa are qualitatively observed to be somewhere between regimes IV and III and within regime III, respectively, but plot completely within regime IV. A better fit exists for Hohenstoffeln 3 MPa, which plots 'correctly' near the IV-III boundary (Fig. 11). However, both Billstein 3 MPa and Sommata 3 MPa visually appear to be within regime III and II, respectively, but on the diagram fall between regime IV and III, and inside regime III.

There are two main explanations for the discrepancies that occur between the observed regimes on the high-speed videos and where the experiments plot on Fig. 11. First, the regime boundaries in the diagram may not be fully applicable to magmas and/or our experimental design, since they were defined from data on diesel sprays used in internal combustion engines (Lefebvre and McDonell, 2017). Specifically, our Weber numbers are higher, because of the larger density, surface tension and jet diameter relative to typical industrial applications. Secondly, our Reynolds numbers are also likely to be different (shifted to lower ranges), because of magma viscosity values between four and five orders of magnitude higher than diesel fuels or water. Determination of jet breakup regime boundaries at higher We values and perhaps lower Re values should be the focus of future work. For example, analogue fluids with rheological behavior, viscosities, densities and

surface tensions similar to our magmas, could be investigated in jet breakup experiments to verify and extend the regime boundaries.

6.2. Jet breakup regimes in Hawaiian eruptions

Rather than dense magma being pushed up and fragmented by suddenly injected pressurized argon gas as in our experiments, in natural lava fountains, a magma column is rapidly accelerated upward by exsolved volatile gases coupled to the magmatic melt (Parfitt, 2004; La Spina et al., 2021). Our experimental transient magma jets last less than 1 s (Zimanowski et al., 1997), whereas natural lava fountains episodes can be sustained for several hours to a few days (Gonnermann and Manga, 2013; Taddeucci et al., 2015). But despite the apparent "steady" appearance of some lava fountain phases, they are actually produced by the fast repetition of discrete pulses Taddeucci et al., 2015). In this regard, our experiments might be regarded as comparable to a single pulse of a lava fountain, and to some extent to an instant in the emission of an industrial liquid jet breaking up within a certain regime.

Strong (i.e., high mass eruption rate), high and narrow lava fountains partly resemble full sprays, hence liquid jets in regime IV. Examples from Hawaii include the Pu'u 'Ō'ō (Kīlauea) 1983 eruption episode 23 (Fig. 12a), or Kīlauea Iki 1959 episodes 1 and 3 (Fig. 12b, c).

Some weaker and lower fountains characterized by a more compact profile might be in regime III, with many clasts forming but an intact (unfragmented) liquid core

near the vent that is either observable or at least plausible (the external fragmented part of the fountain tends to hide the coherent internal part, if present). Examples include Bardarbunga-Holuhraun (Iceland) 2014 (Fig. 12d), or the Lower East Rift Zone (Kīlauea) 2018 fissure 22 (Fig. 12e).

Jet breakup characteristics similar to regime II might be seen where very weak fountains feed lava flows. Fragmentation is coarse, and the weak jet might be largely unfragmented when first exiting the vent. Most clasts probably coalesce back together upon landing. An example is the Lower East Rift Zone (Kīlauea) 2018 fissure 8 (Fig. 12f, g).

Regime I-type jets probably do not occur in Hawaiian eruptions because they would be largely dampened by gravity. So regime I and the even weaker dripping regime are likely replaced by lava oozing from the vent without fragmentation (Parfitt, 2004; Gonnermann and Manga, 2013).

6.3. Controls on natural lava fountains

Although La Spina et al. (2021) focus on high Re as leading to strong lava fountains in their simulations, our work suggests that high We values are also important to reach regime IV. This leads us back to figure 1d, which can be used to qualitatively discuss the controls on natural lava fountains.

6.3.1. Ejection speed

In general, a certain mass discharge rate will be needed to reach and stay within the fountaining style. In the initial stage of a fountain pulse, assuming both conduit diameter and viscosity to be constant, increasing ejection velocity would result in a shift towards the atomization regime (regime IV).

6.3.2. Conduit size

All else being equal including the ejection speed, a larger conduit diameter (and therefore a high mass eruption rate) would favor development of internal turbulence within the flow, and would therefore promote the transition to higher regimes. However if the mass ejection rate is fixed, a smaller conduit favors a higher ejection velocity. This is why fissures that evolve to cylindrical conduits favor fountaining (Jones et al., 2017).

6.3.3. Viscosity

On the contrary, an increase in magma viscosity (e.g., a slightly more silicic chemical composition, or a slightly lower magma temperature) would cause a fountain pulse to begin in a lower regime, with less or no atomization. Alternatively, a magma with a higher viscosity would require a larger ejection velocity in order to produce and sustain a lava fountain, relative to an ultramafic or hot mafic magma.

6.3.4. Bubbles and density

In lava fountains, the abundance of gas bubbles introduces some contrasting phenomena. From a jet breakup perspective, a higher volume fraction of bubbles would decrease the bulk density of the magma, therefore theoretically promoting the transition towards the Rayleigh regime (Fig. 1d). However, this effect of gas bubbles on density is likely cancelled by magma acceleration in the conduit, so that the net effect of more bubbles is probably higher We and Re.

6.3.5. Surface tension

Like in industrial liquids, the hydrodynamic breakup of natural magmas in lava fountains is strongly influenced by surface tension, with which the other internal properties and aerodynamic effects compete. Although surface tension varies only within a limited range in magmas, other variables vary greatly and dictate whether the effects of surface tension will dominate or not. During the climax of large lava fountain episodes, surface tension is overwhelmed by ejection velocity and aerodynamic effects, typical for regime IV (atomization). By contrast, magma fragmentation in relatively low and weak fountaining episodes would be dominated by surface tension.

6.3.6. Temporal evolution and regime transition

Throughout a whole fountaining episode or even eruption, an overall decrease in magma temperature over time combined with increased crystallization and decrease in volatiles would impede late pulses to attain highest breakup regimes

relative to the earlier pulses (Cashman and Scheu, 2015; Taddeucci et al., 2015). Moreover, possible drainback of colder, crystallized and degassed lava into the vent would decrease the overall magma temperature, contributing to the transition to lower regimes (Wallace et al., 1998).

7. Conclusions and outlook

After reviewing the breakup of liquid jets in industrial and commercial applications, we ejected remolten volcanic rocks from a crucible using compressed gas, leading to the formation of transient 'magma' jets. Changing the gas driving pressure and the magma compositions in the experiments led to three different regimes of liquid jet breakup. Our modified Ohnesorge diagram plotting We versus Re and our experimental "fountain pulses" suggest how the relative competition among different internal magma properties and external aerodynamic effects might lead to various jet breakup regimes. Magma viscosity and ejection velocity seem to be the main factors controlling regime transitions, because these parameters can vary by several orders of magnitude. A higher ejection velocity will result in higher internal turbulence and strong external aerodynamic effects, leading to the fine primary breakup of the magma, within the atomization/spray regime. Lower ejection velocities allow surface tension to play a bigger role, dampening atomization. Magma viscosity has the reverse effect: a lower viscosity favors sprays.

A preliminary examination of natural lava fountains suggests that these three regimes might also occur in Hawaiian eruptions. Lava fountain pulses might be potentially regarded as discrete jets with breakup behaviors ranging from regime II (very weak fountains at the head of lava flows) to regime III (moderate fountains with a perturbed but intact liquid core) and regime IV (fully developed sprays in strong fountains).

This study represents only a first, preliminary attempt to characterize jet breakup mechanisms of discrete pulses such as those occurring in lava fountains and Strombolian eruptions. Significant future work is warranted. First, calculating We and Re requires correct input parameters. A key issue is the magma rheological response over milliseconds, at very high deformation rates. Instantaneous viscosity values needed for Re calculations of transient magma jets seem to be different from those obtained through chemical models or viscometer experiments. Then there is potential to further improve our We-Re diagram to better fit conditions in lava fountains. Regime transitions in various conditions including high We and/or low Re could be accessed through fragmentation experiments using analogue liquid materials able to mimic some aspects of magma behavior, minus the challenges involved in working with molten rock. Finally, high-speed video analysis of actual lava fountains could then be used to validate the diagram.

Declaration of competing interest

The authors declare that they have no known competing financial interests or personal relationships that could have appeared to influence the work reported in this paper.

Acknowledgments

This project was funded by a NSERC Discovery Grant to PSR. We thank Jacopo Taddeucci and Lucy Porritt for reviewing a draft of the manuscript. We thank the two anonymous journal reviewers for their constructive comments.

Author contributions

B.Z. and **R.B.** designed and conducted the fragmentation experiments. **P.P.C.** and **P.S.R.** performed the literature review, wrote the initial manuscript, and prepared the figures. All of the authors contributed to the revision of the contents and the improvement of the manuscript.

Author statement

Please find the author statement. Prof. Bernd Zimanowski and Prof. Ralf Büttner designed and conducted the fragmentation experiments. Dr. Comida and Prof. Ross performed the literature review, wrote the initial manuscript and prepared the figures, with an improvement by Dr. Ingo Sonder. All of the authors contributed to the revision of the contents and the improvement of the manuscript.

Declaration of interests

☒ The authors declare that they have no known competing financial interests or personal relationships that could have appeared to influence the work reported in this paper.

References

Birouk, M., Lekic, N., 2009. Liquid jet breakup in quiescent atmosphere: A review. Atomization and Sprays, 19, 501-528.

Büttner, R., Zimanowski, B., Blumm, J., Hagemann, L., 1998. Thermal conductivity of a volcanic rock material (olivine-melilitite) in the temperature range between 288 and 1470 K. J. Volcanol. Geotherm. Res. 80, 293-302.

Büttner, R., Dellino, P., La Volpe, L., Lorenz, V., Zimanowski, B., 2002. Thermohydraulic explosions in phreatomagmatic eruptions as evidenced by the comparison between pyroclasts and products from Molten Fuel Coolant Interaction experiments. J. Geophys. Res. Solid Earth. 107, ECV 5-1 - 5-14.

Büttner, R., Dellino, P., Raue, H., Sonder, I., Zimanowski, B., 2006. Stress-induced brittle fragmentation of magmatic melts: Theory and experiments. J. Geophys. Res. Solid Earth. 111, 1-10.

Caffier, I., 1998. Investigations on the fragmentation of magmatic melt by expanding gas (Unpublished master's dissertation). Physikalisch-Vulkanologisches Labor, Institut für Geologie & Physikalisches Institut, Julius-Maximilians-Universität, Würzburg, Germany.

Calvari, S., Cannavò, F., Bonaccorso, A., Spampinato, L., Pellegrino, A.G., 2018. Paroxysmal Explosions, Lava Fountains and Ash Plumes at Etna Volcano: Eruptive Processes and Hazard Implications. Front. Earth Sci. 6, 1-20.

Cao, X.-K., Sun, Z.-G., Li, W.-F., Liu, H.-F., Yu, Z.-H., 2007. A new breakup regime of liquid drops identified in a continuous and uniform air jet flow. Physics of Fluids. 19, 057103.

Cashman, K.V., Scheu, B., 2015. Chapter 25 - Magmatic Fragmentation A2 - In: Sigurdsson, H., Houghton, B., McNutt, S.R., Rymer, H., Stix, J. (Eds.), Encyclopedia of Volcanoes. Academic Press, USA, pp. 459-471.

Chigier, N., Reitz, R.D., 1996. Regimes of jet breakup and breakup mechanisms (physical aspects). Prog. Astronaut. Aeronaut. 166, 109.

Clasen, C., Phillips, P.M., Palangetic, L., Vermant, J., 2012. Dispensing of rheologically complex fluids: The map of misery. AIChE Journal 58, 3242-3255.

De Astis, G., Lucchi, F., Dellino, P., La Volpe, L., Tranne, C.A., Frezzotti, M.L., Peccerillo, A., 2013. Geology, volcanic history and petrology of vulcano (central aeolian archipelago), Geo. Soc. Mem. pp. 281-349.

Dürig, T., Sonder, I., Zimanowski, B., Beyrichen, H. ,Büttner, R., 2012. Generation of volcanic ash by basaltic volcanism. J. Geophys. Res. Solid Earth, 117, 1-8.

Eggers, J., Villermaux, E., 2008. Physics of liquid jets. Reports on Progress in Physics. 71, 036601.

Gonnermann, H.M., 2015. Magma Fragmentation. Annual Review of Earth and Planetary Sciences, 43: 431-458.

Gonnermann, H.M., Manga, M., 2013. Dynamics of magma ascent in the volcanic conduit. In: R.M.C. Lopes, S.A. Fagents and T.K.P. Gregg (Editors), Modeling Volcanic Processes: The Physics and Mathematics of Volcanism. Cambridge University Press, Cambridge, pp. 55-84.

Hobiger, M., Sonder, I., Büttner, R., Zimanowski, B., 2011. Viscosity characteristics of selected volcanic rock melts. J. Volcanol. Geotherm. Res. 200, 27-34.

Jones, T.J., Llewellin, E.W., Houghton, B.F., Brown, R.J., Vye-Brown, C., 2017. Proximal lava drainage controls on basaltic fissure eruption dynamics. Bull. Volc. 79, 81.

Jones, T.J., Reynolds, C.D., Boothroyd, S.C., 2019. Fluid dynamic induced break-up during volcanic eruptions. Nat. Commun. 10, 1-7.

Koopmann, A., 2004. Magma mingling: die hydrodynamische Genese magmatischer Dispersionen. Dissertation zur Erlangung des naturwissenschaftlichen Doktorgrades der Bayerischen Julius- Maximilans-Universität Würzburg. 148pp

La Spina, G., Arzilli, F., Llewellin, E.W., Burton, M.R., Clarke, A.B., De' Michieli Vitturi, M., Polacci, M., Hartley, M.E., Di Genova, D., Mader, H.M., 2021. Explosivity of basaltic lava fountains is controlled by magma rheology, ascent rate and outgassing. Earth. Planet. Sc. Lett. 553, 116-658.

Lefebvre, A.H., Mcdonell, V.G., 2017. Atomization and sprays. CRC press, Boca Raton, 300pp. https://doi.org/10.1201/9781315120911

Mader, H.M., Llewellin, E.W. ,Mueller, S.P., 2013. The rheology of two-phase magmas: A review and analysis. J. Volcanol. Geotherm. Res. 257, 135-158.

Madlener, K., Frey, B., Ciezki, H.K., 2009. Generalized Reynolds number for non-newtonian fluids. EUCASS Proceedings Series – Advances in AeroSpace Sciences, 1: 237-250.

Mccarthy, M.J., Molloy, N.A., 1974. Review of stability of liquid jets and the influence of nozzle design. The Chemical Engineering Journal 7, 1-20.

Mueller, S.B., Houghton, B.F., Swanson, D.A., Fagents, S.A., Klawonn, M., 2018. Intricate episodic growth of a Hawaiian tephra deposit: case study of the 1959 Kīlauea Iki eruption. Bull. Volc. 80, 1-19.

Murase, T., McBirney, A.R., 1973. Properties of some common igneous rocks and their melts at high temperatures. Geol. Soc. Am. Bull. 84, 3563-3592.

Parfitt, E.A., 2004. A discussion of the mechanisms of explosive basaltic eruptions. J. Volcanol. Geotherm. Res. 134, 77-107.

Parfitt, E.A., Wilson, L., 2009. Fundamentals of physical volcanology. John Wiley & Sons.

Reitz, R.D., Bracco, V.F., 1986. Mechanism of breakup of round liquid jets. Encyclopedia of fluid mechanics, 10.

Sallam, K.A., Aalburg, C., Faeth, G.M., 2004. Breakup of Round Nonturbulent Liquid Jets in Gaseous Crossflow. AIAA Journal. 42, 2529-2540.

Shimozuru, D., 1994. Physical parameters governing the formation of Pele's hair and tears. Bull. Volc. 56, 217-219.

Sonder, I., Zimanowski, B., Büttner, R., 2006. Non-Newtonian viscosity of basaltic magma. Geophys. Res. Lett. 33.

Taddeucci, J., Edmonds, M., Houghton, B., James, M.R., Vergniolle, S., 2015. Chapter 27 - Hawaiian and Strombolian Eruptions A2 - In: Sigurdsson, H., Houghton, B., McNutt, S.R., Rymer, H., Stix, J. (Eds.), Encyclopedia of Volcanoes. Academic Press, USA, pp. 485-503.

Walker, D., Mullins, O., 1981. Surface tension of natural silicate melts from 1,200°–1,500° C and implications for melt structure. Contrib. Mineral. Petr. 76, 455-462.

Wallace, P.J., Anderson Jr., A.T., 1998. Effects of eruption and lava drainback on the H2O contents of basaltic magmas at Kilauea Volcano. Bull. Volc. 59, 327-344.

Wallace, P.J., Plank, T., Edmonds, M. ,Hauri, E.H., 2015. Chapter 7 - Volatiles in Magmas - In: Sigurdsson, H., Houghton, B., McNutt, S.R., Rymer, H., Stix, J. (Eds.), Encyclopedia of Volcanoes. Academic Press, USA, pp. 163-183.

Wang, X.-H., Huang, Y., Wang, S.-L., Liu, Z.-L., 2012. Bag Breakup of Turbulent Liquid Jets in Crossflows. AIAA Journal. 50, 1360-1366.

Zimanowski, B., Fröhlich, G., Lorenz, V., 1991. Quantitative experiments on phreatomagmatic explosions. J. Volcanol. Geotherm. Res. 48, 341-358.

Zimanowski, B., Fröhlich, G., Lorenz, V., 1995. Experiments on steam explosion by interaction of water with silicate melts. Nucl. Eng. Des. 155, 335-343.

Zimanowski, B., Büttner, R., Lorenz, V., Häfele, H.G., 1997. Fragmentation of basaltic melt in the course of explosive volcanism. J. Geophys. Res. Solid Earth. 102, 803-814.

Zimanowski, B., Büttner, R., Koopmann, A., 2004. Experiments on magma mixing. Geophys. Res. Lett. 31, L09612 09611-09613.

Zimanowski, B., Büttner, R., Dellino, P., White, J.D.L., Wohletz, K.H., 2015. Chapter 26 - Magma–Water Interaction and Phreatomagmatic Fragmentation A2 - In: Sigurdsson, H., Houghton, B., McNutt, S.R., Rymer, H., Stix, J. (Eds.), Encyclopedia of Volcanoes. Academic Press, USA, pp. 473-484.

Fig. 1. Four liquid jet breakup regimes occur in industrial applications: I – Rayleigh regime, II – First wind-induced regime, III – Second wind-induced regime, IV – Atomization regime. (a) Jet stability curve displaying the relationship between intact length before primary breakup and ejection velocity of the liquid jet; after Lefebvre and McDonell (2017). (b) Visual representation of the liquid jet within each regime, for a jet issued downward in a stagnant atmosphere. One way to transition from one regime to another is to change the ejection velocity, which corresponds to different intact length for primary breakup (vertical red bars); after Chigier and Reitz (1996) and Lefebvre and McDonell (2017). (c) Traditional Ohnesorge classification determined through the relationship between the Ohnesorge and Reynolds numbers; after Lefebvre and McDonell (2017). (d) Modified “Ohnesorge” diagram showing the Weber and Reynolds numbers. Colored arrows illustrate the effect of varying the main parameters. The power decay of the regime boundaries is ~ $Re^{-0.5}$.

Fig. 2. Magma compositions and experimental setups. (a) Total alkalis vs. silica diagram (Le Bas et al., 1986). Data for Hohenstoffeln and Sommata from Hobiger et al. (2011) and Billstein from Zimanowski et al. (2004). (b) Schematic drawing of the “high-speed” (10 MPa) blowout type experiment setup. (c) Schematic drawing of the “low-speed” (3 MPa) injection type experiment setup. Schemes modified from Austin-Erickson et al. (2008). (d) Frame of an experiment run (Billstein 10 MPa) at the beginning of the free air expansion, showing the portion of the melt affected by gas piercing (on the left) and the still coherent portion of the melt plug (on the right).

Fig. 3. Physical properties of the tested magmas. (a) Temperature-dependent surface tensions of Hohenstoffeln (olivine-melilitite) and Billstein (alkaline basalt) magmas, along with other reference materials: i) Columbia River (basalt), ii) Mt. Hood (andesite), iii) Newberry (rhyolite). Surface tension for all material shows little variation at 1200°C. (b) Bubble-free density versus silica for Hohenstoffeln and Sommata (basaltic trachyandesite), along with other reference materials: i) Galápagos (olivine basalt), ii) Columbia River (basalt), iii) Mt. Hood (andesite), iv) Newberry (rhyolite). It can be assumed that Billstein has an intermediate density between Hohenstoffeln and Sommata, similar to Galápagos. (c) Viscosity versus silica trends for the tested magmas at 1200°C. Vertical lines show the effect of different shear rates on equilibrium viscosities in viscometry experiments; Data sources: (1) Koopmann (2004); (2) Murase and McBirney (1973); (3) Walker and Mullins (1981); (4) Büttner et al. (1998); (5) Büttner et al. (2002); (6) Hobiger et al. (2011); (7) Sonder et al. (2006).

Fig. 4. Initial movement of the magma plug and in-crucible fragmentation for the blowout-type setup. At t0, pressurized argon gas is injected at the base of the magma. Rayleigh-Taylor instabilities appear at the gas-magma interface. At t1, the wave disturbances reach a critical amplitude, and droplets are detached. This continues until the disturbed magma plug surpasses the crucible opening. In-crucible fragmentation depends on driving pressure and magma composition.

Fig. 5. Time-lapse of the Hohenstoffeln 10 MPa run, emphasizing the entire free-air fragmentation and expansion of the magma. Time between each frame is 4 ms from the first appearance of the magma front at the crucible opening, plus a special frame at 1 ms to show the location of the gas piercing and coherent portions of the magma plug.

Fig. 6. Time-lapse of the Hohenstoffeln 3 MPa run. Time between each frame is 5 ms, plus a special frame at 3 ms to show the location of the gas piercing and coherent portions of the magma plug.

Fig. 7. Time-lapse of the Billstein 10 MPa run. Time between each frame is 4 ms, plus a special frame at 2 ms to show the location of the gas piercing and coherent portions of the magma plug.

Fig. 8. Time-lapse of the Billstein 3 MPa run. Time between each frame is 5 ms, plus a special frame at 1.6 ms to show the location of the gas piercing and coherent portions of the magma plug.

Fig. 9. Time-lapse of the Sommata 10 MPa run. Time between each frame is 4 ms, plus a special frame at 2 ms to show the location of the gas piercing and coherent portions of the magma plug.

Fig. 10. Time-lapse of the Sommata 3 MPa run. Time between each frame is 5 ms, plus a special frame at 3 ms, although for this run that was no visible gas piercing effect.

Fig. 11. Modified “Ohnesorge” diagram showing the Weber and Reynolds numbers, applied to the early stage of the jet phase during free air expansion, for each experimental run. See text and Table 1 for how each experiment was positioned on this diagram.

Fig. 12. Potential examples of breakup regimes in lava fountains: (a)-(c), regime IV, (d)-(e) regime III, (f)-(g) regime II. (a) Episode 23, Pu'u 'Ō'ō eruption (Kīlauea), July 28, 1983 (Hawaii, U.S.A). Credit: U.S. Geological Survey/photo by J.D. Griggs. (b) Episode 1 of the Kīlauea Iki eruption, November 18, 1959 (Hawaii, U.S.A). Credit: U.S. Geological Survey. (c) Episode 3 of the same eruption, November 29, 1959. Credit: U.S. Geological Survey. (d) Bardarbunga-Holuhraun eruption, September 13, 2014 (Iceland). Credit: Tom Pfeiffer / www.volcanodiscovery.com (used with permission). (e) Fissure 22, Lower East Rift Zone (Kīlauea), May 21, 2018 (Hawaii, U.S.A). Credit: U.S. Geological Survey. (f) Fissure 8, Lower East Rift Zone (Kīlauea), (Left) June 7, 2018. (g) Same eruption, June 9, 2018. Credit: U.S. Geological Survey.

Table 1 Physical parameters of the magma plug among different experiments, for the purpose of calculating the Weber and Reynolds numbers during the early stage of the jet phase, and observed breakup regime on high-speed videos

Run	Crucible diameter (m)	Surface tension (N/m)	Density (kg/m^3)	Ejection velocity (m/s)[1]	Dynamic viscosity range (Pa*s)	Weber number	Reynolds number[3]	Observed regime
10 MPa series	-	-	-	-	-	-	-	-
Hohenstoffeln	0.05	~0.33	~2920	44	21 – 343	8.6 x 10^5	523 – 8547	IV
Billstein	0.05	~0.33	~2700[2]	33	28 – 322	4.5 x 10^5	530 – 6097	IV-III
Sommata	0.05	~0.33	~2500	26	45 – 106	4.9 x 10^5	109 – 257	III
3 MPa series	-	-	-	-	-	-	-	-
Hohenstoffeln	0.05	~0.33	~2920	11	21 – 343	5.4 x 10^4	77 – 1251	IV-III
Billstein	0.05	~0.33	~2700[2]	11	28 – 322	5.0 x 10^4	109 – 1257	III
Sommata	0.05	~0.33	~2500	13	45 – 106	6.4 x 10^4	35 – 83	II

([1]) Values of ejection velocity refer to the coherent portion of the magma plug upon exiting the crucible

([2]) Density of a similar magma composition at 1200°C (Galápagos alkali-olivine basalt, Murase and McBirney, 1973)

([3]) For power-law fluids, calculated using Re_{pl} (from Madlener et al., 2009)

Graphical abstract

Please find below the highlights of the work.

- Lava fountain pulses can be regarded as transient jets of magma
- Jet breakup regimes might occur in lava fountains, similar to classic liquid jets
- Viscosity and ejection velocity of the magma control hydrodynamic breakup processes